JOTCS B
Journal of the Turkish Chemical Society
Section: B
Chemical Engineering
TURKISH CHEMICAL SOCIETY

Evaluation of the Process Parameters on Subcritical Water Gasification of Sorghum by Response Surface Methodology

Açelya Seçer[*a], Ertürk Şayan[a], Şefika Türker Üzden[a], Arif Hasanoğlu[a]

[a]Department of Chemistry, Çukurova University, 01330, Adana, Turkey

Abstract: In this study response surface methodology (RSM) with Box-Behnken design (BBD) was used to evaluate the effects of process parameters of reaction time, initial water volume, amount of feedstock, and amount of catalyst on total gasification and hydrogen production yield by low temperature hydrothermal gasification of Sorghum biomass at 250 °C. Ruthenium(III) chloride was used as a catalyst in catalytic runs. Significances of the main and interacting effects of independent parameters were determined by ANOVA. Numerical optimization was used to optimize the process parameters for maximum yield hydrogen production. The optimum conditions for maximum hydrogen production were determined as a residence time of 58.6 min, water volume of 24.5 mL, and catalyst amount of 0.02 g.

Keywords: Biomass, hydrothermal gasification, hydrogen, response surface methodology, Box-Behnken Design.

Submitted: July 18, 2019. **Accepted:** December 17, 2020.

Cite this: Seçer A, Şayan E, Türker Üzden Ş, Hasanoğlu A. Evaluation of the Process Parameters on Subcritical Water Gasification of Sorghum by Response Surface Methodology. JOTCSB. 2021;4(1):1–12.

***Corresponding author. E-mail:** acsecer@cu.edu.tr.

INTRODUCTION

Most of the energy need is still met by conventional fossil fuels and the increase in world energy demands results a decrease in traditional energy resources. Also, carbon emission from fossil fuels is a dramatic environmental problem growing day by day and becoming more dangerous. The threat of global warming associated with the increase in greenhouse gas emissions, such as CO_2, has increased the number of research on this issue, and most of the work is particularly related to the development of technologies to reduce these emissions. These effects, combined with declining reserves of conventional sources, necessitated the use of sustainable new generation energy sources, which would replace the old ones (1). Hydrogen, which has the potential to solve these major problems as it can be utilized without any environmental impacts, is a good alternative among the new generation energy fuels. It is not a primary energy source but can be produced from another source to be transformed for later uses. Therefore, hydrogen production technologies are among the most studied and developed technologies in recent years (2). Among these technologies, hydrogen production from biomass has some advantages over others as biomass is abundant and totally renewable (3). Lignocellulosic biomasses are the most abundant and economical raw materials as they can easily be grown in almost all conditions. Their cellulose and hemicellulose contents can also be modified and enriched (4). Furthermore, since the amount of CO_2 that these plants take from the atmosphere by photosynthesis to grow is the same as the amount of CO_2 released when they processed, the net effect of biomass processing on CO_2 emissions is zero. These advantages make lignocellulosic biomass a very good alternative energy source in environmental and economic terms. However, since there is too much moisture in the biomass structure, it may need to be dried for use in some processes, which leads to an increased cost of the processes. In this process, water is a participant of the system and acts as both the reaction medium and the reactant, and thus does not need to be removed from the medium (5). Properties of water at different temperature and

pressures are different than those of water under normal conditions and the water amount directly affects the system pressure. So that, water amount, reaction temperature and system pressure are the key parameters affecting the system performance and the product gas distributions (6). Also different types of catalysts can also be used in hydrothermal gasification for specific purposes at different conditions (7–11). Gasification process is a process in which many factors have some effects at the same time, and the relations of these effects with each other are as important as their individual effects. Therefore, a method in which each of these effects can be examined together with the interacting effects can be very useful for the development of the process. Response surface methodology (RSM) is defined as a method in which statistical and mathematical techniques are used together for development and optimization of processes (12). The relationship between one or more response variables and a set of quantitative parameters can be examined with a response surface method called Box–Behnken design (BBD). It is a variety of rotational designs from incomplete multi–factor designs, which are used in the estimation of second order model parameters. The number of test points for BBD is determined by the "N= 2k(k–1) + nc" equation where "k" indicates the number of factors and "nc" indicates the number of central attempts (13,14). Because the lower and upper limits for all factors in design are never covered at the same time, unsatisfactory results from extreme values are prevented by BBD. The experimental designs have fewer design points and fewer experiments to be performed. Examples of the use of the method in gasification can be found in the literature (15–19).

In this study, we perform the hydrothermal gasification of sorghum at 250 °C and evaluate the individual and simultaneous effects of residence time, initial water volume, amount of biomass, and amount of catalyst in terms of hydrogen production with RSM combined with BBD. In a previous study, we performed the gasification of kenaf biomass at sub-critical conditions at temperatures from 250 to 325 °C, and obtained a maximum H_2 mole fraction in the gaseous product (44.5%) at 250 °C with $RuCl_3$ catalyst (20). So in this study the temperature was kept constant at 250 °C. In this way the gasification process was performed and evaluated at milder conditions than traditional ones for better energy efficiency. Since the traditional studies can only deal with the individual factor effects, this study also brings novelty to the literature by not only determining the individual effects of independent parameters on gasification performance but also understanding the interacting process parameters. Numerical optimization was used to optimize the process parameters for maximum hydrogen yield. The factors affecting hydrogen production from gasification of sorghum under these conditions were examined together, as well as how the factors could be modified according to each other to achieve the desired result under the desired specific conditions. In addition, the most suitable conditions for hydrogen production could be determined by 95% confidence level with few experiments.

MATERIALS AND METHODS

Materials

Sorghum is used as lignocellulosic biomass which was ground to pass 140 meshes. Moisture, ash and elemental analysis results of sorghum biomass are given in Table 1. Anhydrous Ruthenium(III) chloride (99%, J&K) was used as the catalyst in catalytic runs.

Table 1. Moisture, ash and elemental analysis results of sorghum biomass .

	Sorghum
C (wt %, dry)	39.8
N (wt %, dry)	0.8
H (wt %, dry)	5.2
S (wt %, dry)	N/A
O (wt %, dry)[a]	45.8
Moisture (wt %)	8.1
Ash (wt %, dry)	8.4
Volatile matter (wt %, dry)	nd
Fixed carbon (wt %, dry)	nd

[a]: calculated from difference; nd: not determined

Method

Gasification experiments

Sorghum biomass was gasified at 250 °C. The gasification of biomass was performed in a 100 mL stainless steel high pressure reactor (PARR Model 4590 micro bench type) equipped with magnetic drive stirrer and temperature controller system. The desired amount (dry, ash–free basis) of sorghum biomass and catalyst (in experiments where the catalyst is used) was placed in the reactor with the desired volumes of water which was stated in the experimental plan. Then the reactor was purged with Argon for air removal and sealed. Argon gas was sent to the system with a continuous input and output during purge process. The relevant pressures were monitored to confirm that there was no amount of gas left in the reactor that would affect the gasification results. Reactor temperature was

raised to 250 °C starting from the room temperature and gasification was continued for the time specified in the experimental plan by stirring at 1000 rpm continuously via the magnetic–drive. The internal (autogenous) pressure inside the reactor was observed between 100–350 psi depending on the amount of initial water used. At the end of the process the reactor was taken out of the heating system and was immediately cooled down to room temperature using an ice–cold water mixture.

Gas and liquid product analysis

Gaseous products were collected into a gas buret that was filled with water and the total gas volume was measured by water displacement. A dual–channel Varian 450 series GC equipped with two TCD detectors were used for product characterization. Remaining liquid products were transferred into a cellulose thimble with dichloromethane and extraction method was applied using dichloromethane solvent and analyzed with Gas Chromatography–Mass Spectrometry (GC–MS) to obtain detailed chemical compositions. GC–MS analysis was performed by Thermo Finnigan GC–MS using Thermo TR-5MS capillary column (60 m x 0.25 mm ID x 0.25 µm). Detailed information about gas and liquid product analysis were given in previous studies (21).

Experimental design and optimization

A 4–factor and 3–level design was performed by Design Expert 12 software to evaluate the effects of performance parameters of reaction time (min), water volume (mL), amount of feedstock (g), and amount of catalyst (g) and to optimize these parameters for maximum hydrogen production. Total volume, hydrogen and carbon dioxide volumes produced after gasification were used for response factors. The independent variables were coded as follows; “A” for reaction time %, “B” for water volume, “C” for biomass amount and “D” for catalyst amount. The low, center, and high levels of each factor level were donated as –1, 0 and +1, respectively. Experimental range levels of the independent variables were given in Table 2. 15 experiments were performed in a randomized order. A quadratic equation (Eq. 1) was used to establish a mathematical relationship between the variables and the response;

$$Y=\beta_0+\sum_{i=1}^{N}\beta_i\times X_i+\sum_{i=1}^{N}\beta_{ii}\times X_i^{\,2}+\sum_{i=1}^{N-1}\sum_{j=i+1}^{N}\beta_{ij}\times X_{ij} \quad \text{(Eq. 1)}$$

where Y is the predicted response, N is the number of variables, X_i is the independent variable, β_0, β_i, β_{ii}, and β_{ij} are the intercept terms, the linear effect, the squared effect and the interaction effect, respectively (22).

Table 2. Experimental range and levels of the independent variables.

Variables	Factor	Range and Level		
		–1	0	1
Time (min)	A	0	50	100
Water volume (mL)	B	0	35	70
Biomass amount (g)	C	1	4	6
Catalyst amount(g)	D	0.01	0.10	0.20

RESULTS AND DISCUSSION

The effects of four factors, namely reaction time (F1), initial water volume (F2), amount of catalyst (F3), and amount of biomass (F4) on hydrothermal gasification sorghum biomass at 250 °C were evaluated by employing Box-Behnken designed RSM. The experimental points, in coded and actual values, with observed response values were given in Table 3. The l results were determined by using analysis of variance (ANOVA) statistically. The term “A” is coded for reaction residence time (min); “B” is for the volume of water (mL) in the reactor, “C” is for biomass weight used (g), and “D” is for amount of catalyst (g).

Table 3. Experimental plan and the observed response values.

	Experimental plan								Observations		
	F1	F2	F3	F4					R1	R2	R3
Run number	Residence time	Water volume	Biomass	Catalyst	A	B	C	D	Total gas	H_2	CO^2
	min	mL	g	g					mL	mL	mL
1	-1	0	-1	0	15	15	1	0.11	126.0	53.5	62.8

2	-1	0	1	0	15	15	6	0.11	558.0	187.5	340.9
3	1	0	-1	0	60	15	1	0.11	166.5	54.0	30.8
4	1	1	0	0	60	30	4	0.11	325.5	115.2	169.9
5	0	0	0	0	38	15	4	0.11	349.0	112.9	196.5
6	0	-1	1	0	38	0	6	0.11	557.0	114.0	312.8
7	0	0	-1	-1	38	15	1	0.01	126.0	57.7	59.8
8	0	0	0	0	38	15	4	0.11	357.0	115.0	204.4
9	1	-1	0	0	60	0	4	0.11	380.0	113.9	224.4
10	0	-1	0	-1	38	0	4	0.01	380.0	128.6	211.6
11	0	0	-1	1	38	15	1	0.20	107.1	38.6	57.1
12	0	-1	0	1	38	0	4	0.20	325.5	43.8	220.5
13	0	0	1	-1	38	15	6	0.01	660.0	226.0	399.0
14	-1	0	0	1	15	15	4	0.20	650.0	134.0	88.0
15	0	0	0	0	38	15	4	0.11	423.3	81.3	246.2
16	0	1	-1	0	38	30	1	0.11	76.0	3.8	66.5
17	0	-1	-1	0	38	0	1	0.11	162.9	59.0	187.2
18	1	0	1	0	60	15	6	0.11	528.1	196.5	263.1
19	0	1	0	-1	38	30	4	0.01	354.0	48.0	191.0
20	0	0	0	0	38	15	4	0.11	380.6	91.0	119.5
21	0	0	0	0	38	15	4	0.11	236.0	82.5	148.9
22	-1	0	0	-1	15	15	4	0.01	308.5	126.0	171.0
23	0	1	1	0	38	30	6	0.11	444.1	122.3	303.7
24	-1	-1	0	0	15	0	4	0.11	465.5	133.0	237.6
25	-1	1	0	0	15	30	4	0.11	199.5	43.0	157.8
26	1	0	0	1	60	15	4	0.20	309.2	56.5	146.7
27	0	0	1	1	38	15	6	0.20	532.5	98.4	216.8
28	1	0	0	-1	60	15	4	0.01	460.0	183.8	251.3
29	0	1	0	1	38	30	4	0.20	253.0	37.1	194.6

Effects of process parameters total gas volume

The significance of the effects of input process variables (reaction residence time, "initial volume of water (mL) in the reactor, biomass weight used and amount of catalyst) and their interactions on total gas volume at 250 °C were determined by ANOVA. The results are given in Table 4. Values of coefficients of determination (R^2) statistically measures how close the data are to the fitted regression line and the strength of the relationship between the model and a variable. The values of R^2 for the responses of pressure were also given in Table 4. The values of R^2 and adjusted R^2 were calculated as 0.9136 and 0.8272. Predicted R-squared is a measure of how well the model predicts a response value. It helps to determine the overfitting a regression model. An over fit model includes an excessive number of terms, and it begins to fit the random noise in the sample. A predicted R-squared that is distinctly smaller than R-squared is a warning sign for overfitting. It is computed as:

$$Pred.R^2 = 1 - \left[\frac{PRESS}{SS_{residual} + SS_{model}}\right] = 1 - \left[\frac{PRESS}{SS_{total} - SS_{curvature} - SS_{block}}\right] \quad \text{(Eq.2)}$$

PRESS is the "predicted residual sum of squares" for the model. A measure of how well a particular model fits each point in the design. The coefficients for a new model are calculated with one point "deleted". The new model's prediction is subtracted from the "deleted" observation to find the predicted residual.

This is done for each data point. The predicted residuals are squared and added together to form the PRESS. The Adjusted R-squared and Predicted R-squared should be within approximately 0.20 of each other to be in “reasonable agreement.” If they are not, there may be a problem with either the data or the model (23).

The Predicted R^2 of 0.7133 is in reasonable agreement with the adjusted R^2 of 0.8272; i.e. the difference is less than 0.2. These results indicated that the proposed equation was appropriate to evaluate the relationship of total gas volume with the input variables without overfitting.

Table 4. ANOVA results for total gas volume.

Source	F-value	p-value
Model	10.57	< 0.0001
A-time (min)	0.3525	0.5622
B-water volume (mL)	7.06	0.0188
C-weight of biomass (g)	116.63	< 0.0001
D-weight of catalyst (g)	0.2279	0.6405
AB	2.48	0.1380
AC	0.2745	0.6086
AD	13.41	0.0026
BC	0.0375	0.8492
BD	0.1197	0.7346
CD	0.6529	0.4326
A^2	1.54	0.2356
B^2	1.91	0.1884
C^2	0.6549	0.4319
D^2	1.41	0.2547
Lack of Fit	0.9076	0.5925
R^2	0.9136	
Adjusted R^2	0.8272	
Predicted R^2	0.7133	

The empirical model defining the relative impact of the input variables on total gas volume in terms of coded values is shown below;

$$Y_1 = (349.2 - 11.5A - 51.8B + 209.6C - 9.26D + 52.9AB - 17.6AC - 123.1AD - 6.51BC - 11.6BD - 27.2CD + 32.7\,A^2 - 36.5B^2 - 21.4C^2 + 31.4) \times D^2 \quad \text{(Eq. 3)}$$

where Y_1 represents the total gas volume. The factor coefficients give ideas about the relative effects of the factors on the desired response. The negative sign of a coefficient indicates that the increasing levels of the factor cause decreases in the desired response values whereas the positive sign means an increasing effect of the coefficient on the desired response in contrast.

According to ANOVA results, the Model F–value was 10.57 with a very low p value (<0.0001), which implied that the overall model is significant for the response of total gas volume. Hence, the model can be used to express the significance of the model parameters. P-values less than 0.0500 indicate model terms are significant, in this case B, C, AD are significant model terms. The model term “B” represents the initial water volume in the reactor and found to have a significant effect on total gas yield. The direction of the effect was found to be negative in equation 3 which means the increasing initial volumes of water used in the process will cause decreases in total gas volume obtained in the process. The direction of the individual effect of the water volume factor was graphically expressed by the one factor graph of total gas volume as a function of water volume in Figure 1(a). The pressure–temperature behavior of water in closed systems has been studied by Laudise (24). When the vessel was filled initially with water to less than 32% of the vessel capacity, the liquid level drops as the temperature increases because the liquid is lost, i.e. the water boils to dry. If the vessel is filled initially with water to 32%, the liquid level remains unchanged as the temperature rises. In the case of the loss of liquid to the vapor phase is exactly balanced by the liquid volume expansion. In a closed vessel filled more than 32% with water, the liquid will expand to completely fill the vessel at some temperature below the critical temperature. The higher the filling percentage, the lower the temperature at which the phase in the vessel becomes liquid (24). As the volume of water is increased, the volume of vapor decreases and the volume of liquid phase increase in the reactor. All these changes observed in the liquid-vapor phase levels of the system depending on the gasification conditions lead to changes in product distribution and gasification yields (20). Therefore, in a closed system, the vapor and its level In general, gas–gas and gas–solid reactions occur faster than liquid–liquid and liquid–solid reactions. In experiments where lower volumes of water were used, probably the gas–gas and gas–solid reactions are more likely to be more effective and the process becomes more efficient than the experiments in which higher volumes of water were used (20).

The other significant and effective model term “C” represents the weight of biomass to be gasified, and the positive sign of “C” in equation indicates that the direction of the effect is positive. Figure 1(b) also shows that the increased amount of biomass leads to an increase in total gas volume.

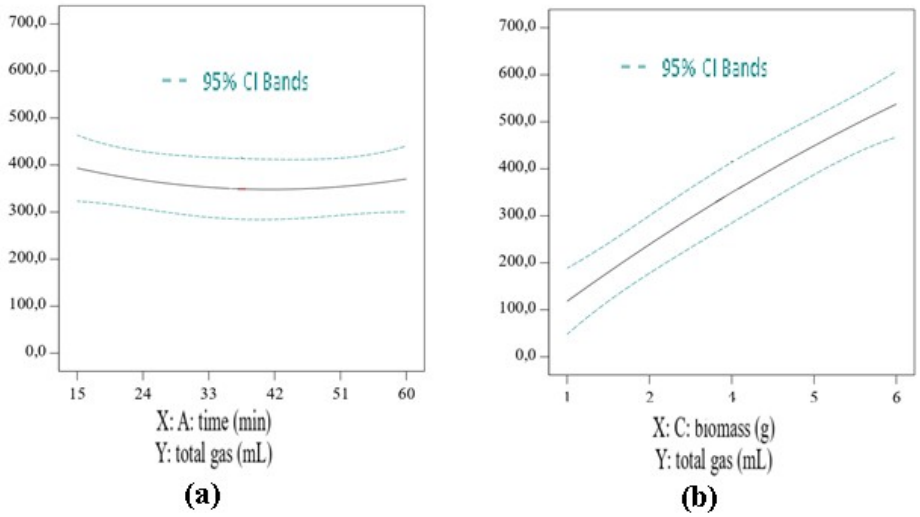

Figure 1. Total gas volumes (mL) as function of a) reaction time (min) b) biomass amount (g).

An interaction effect is the simultaneous effect of two or more independent factors on at least one desired response in which their joint effect is significantly greater (or significantly less) than the sum of the parts. Here, the significant term "AD" expresses the interaction effect between the residence time and amount of catalyst. As the coefficient factor of AD in equation is relatively higher, it can be said that this interaction affects the total gas production more than other factors. Also the direction of the effect is negative. To have more information about the effects of this interaction, the interaction graph (Figure 2(a)) and 3-dimensional (3D) response surface plots of total gas volume against residence time and catalyst amount (Figure 2(b)) can be examined.

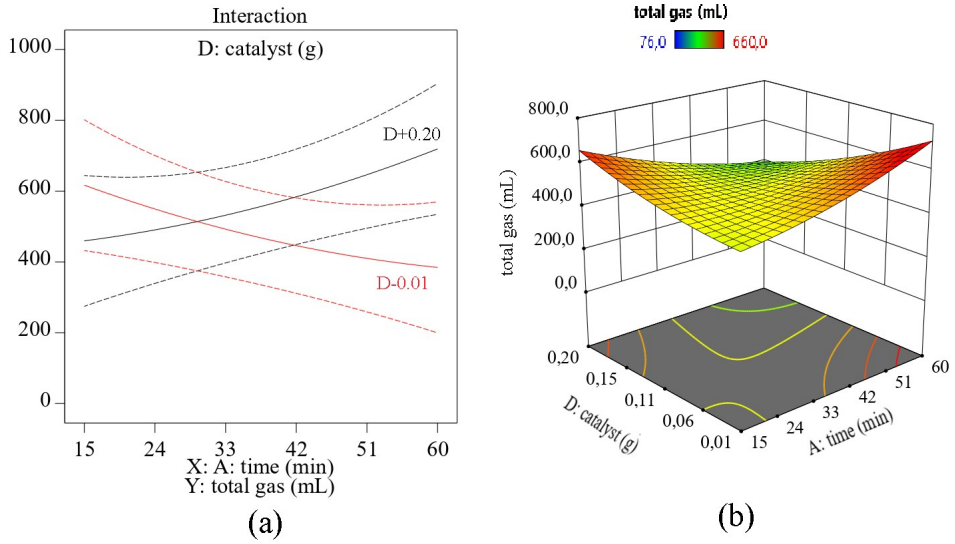

Figure 2. (a) Interaction graph of reaction time and catalyst amount (b) 3D response surface plot of total gas volume as function of catalyst amount and reaction time.

According to the information given by the interaction graphs, while the increase in the reaction times at the low levels of catalyst (D-0.01) caused a decrease in the total volume, the lower the reaction times and the higher the total gas volume production at higher catalyst amount levels (D+0.02). This result shows that the reaction time can be shortened by increasing the amount of catalyst, or the reaction times should be kept longer if a high amount of gas is desired by using lower amounts of catalyst. Since the reaction rate of hydrolysis in subcritical water is slower than that in supercritical water (25), it is difficult to gasify high molecular weight constituents of biomass such as cellulose and lignin. However, it is advantageous to gasify biomass in this temperature region since the

input thermal energy would be low even though the gasification rate would be slow. This means that the role of the catalyst in low temperatures becomes important (7). Many catalysts such as nickel, ruthenium, palladium, platinum and rhodium have been examined and reported to be effective to increase the gasification performances at subcritical gasification conditions. (9).

Although the gaseous products formed after experiments are mixtures of H_2, CO_2, CO and CH_4, the major products are hydrogen and carbon dioxide, even CO_2 has the greatest ratio almost in all runs (37-71%). H_2 contents vary from 15% to 55% whereas the CO and CH_4 contents vary between 1% and 10%. No significant correlations between the process parameters and the CO and CH_4 contents of the product gas can be found, so only the effects of process parameters on hydrogen and carbon dioxide production will be evaluated in this study.

Effects of process parameters on H_2 yield and CO_2 production

The ANOVA results showing the significance of the process parameters and on hydrogen production and R^2 values are given in Table 5. The values of R^2 and adjusted R^2 were calculated as 0.9502 and 0.9003. The Predicted R^2 of 0.7681 is in reasonable agreement with the adjusted R^2. These results indicated that the proposed equation was appropriate to evaluate the relationship of hydrogen volume with the input variables.

Table 5. ANOVA results for hydrogen volume and carbon dioxide volume.

	H_2		CO_2	
Source	F-value	p-value	F-value	p-value
Model	19.06	< 0.0001	7.76	0.0002
A-time (min)	0.5294	0.4789	0.0341	0.8562
B-water volume (mL)	14.26	0.0020	1.93	0.1861
C-weight of biomass (g)	132.03	< 0.0001	94.36	< 0.0001
D-weight of catalyst (g)	37.55	< 0.0001	5.64	0.0324
AB	7.19	0.0179	0.0836	0.7767
AC	0.0617	0.8075	0.2734	0.6092
AD	15.76	0.0014	0.0609	0.8087
BC	3.48	0.0833	0.0176	0.8963
BD	4.70	0.0479	0.0036	0.9527
CD	10.13	0.0067	4.21	0.0593
A^2	16.78	0.0011	0.3073	0.5881
B^2	16.28	0.0012	1.31	0.2724
C^2	0.3967	0.5389	0.0217	0.8850
D^2	0.0002	0.9882	0.0093	0.9244
Lack of Fit	1.12	0.4985	0.6904	0.7116
R^2	0.9502		0.8858	
Adjusted R^2	0.9003		0.7717	
Predicted R^2	0.7681		0.5882	

The empirical model defining the relative impact of the input variables on hydrogen volume in terms of coded values is shown below;

$Y_2 = 96.6 + 3.6A - 18.6B + 56.2C - 30.1D + 22.8\,AB + 2.1AC - 33.8AD + 15.9BC + 18.5BD - 27.1CD + 27.4A^2 - 27.0B^2 + 4.2C^2 + 0.1D^2$ (Eq. 4)

where Y_2 represents the hydrogen volume.

According to ANOVA B, C, D, AB, AD, BD, CD, A^2, B^2 are significant model terms on hydrogen production since the p-values are lower than 0.05. Water volume (B) was found to be effective on hydrogen production as water is one of the main actors of the hydrothermal process. The direction of the effect seems negative as the factor coefficient of B is negative in Eq. 3. Besides the main effect, water volume is also an interacting parameter the reaction time and catalyst amount, so the certain effect of the water volume factor should be evaluated in terms of so the effect of water volume on hydrogen production should be evaluated by taking into account these interactions. Figure 3(a) and (b) show the 3D surface plots of hydrogen volume as a function of water volume/reaction time and water volume/catalyst amount.

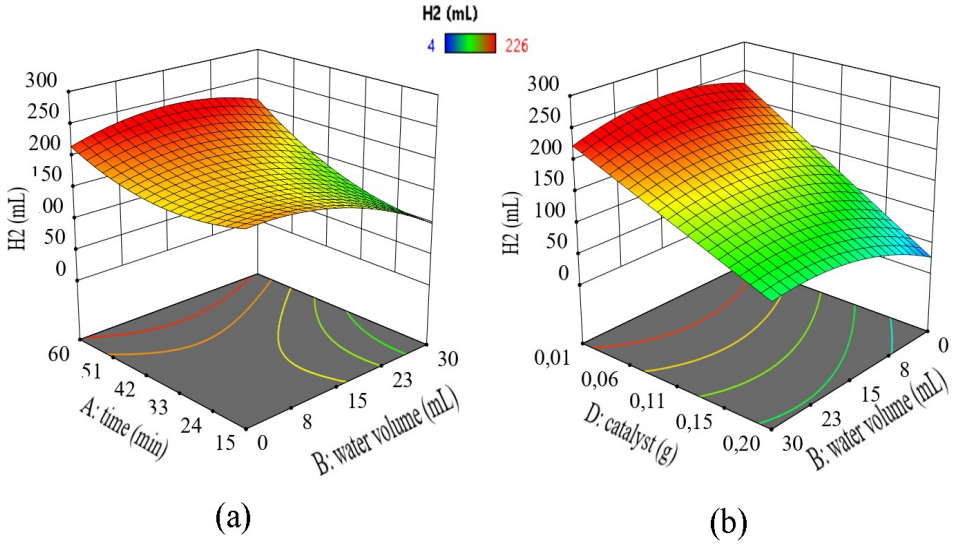

Figure 3. 3D response surface plots of hydrogen volume as function of (a) reaction time (min)/water volume (mL); (b) catalyst amount (g)/water volume (mL).

The relationship between volume and reaction time from Figure 3(a) shows that the increase in hydrogen volume with the increasing reaction time is higher at the highest levels of water volume and reaction time is an effective parameter to reach higher yields of hydrogen. On the other hand, reaction time becomes less effective and there is no significant difference between the hydrogen volumes produced in any reaction time at the lower levels of water volume. This result may indicate that gasification reactions occur rapidly at low water volumes and the effect of the reaction period becomes insignificant. Thus reaction time for such conditions can be kept less provided that the water volume is reduced in order to achieve higher hydrogen yields.

Figure 3b shows the interactions of the water volume with the catalyst amount. It is seen from the figure that more hydrogen is produced at lower levels of catalyst. While the amount of water at the lower levels does not have a significant effect on the volume of hydrogen gas produced, the volume of hydrogen gas tends to increase slightly up to a level of water volume, but tends to decrease slightly after this level. The increase in the amount of catalyst results in a reduction in hydrogen production. Catalyst amount is a significant process parameter in terms of its main effect and negativity of the direction of this effect can also be seen in the Eq. 4 from the negative sign of the factor coefficient “D”. But the effect of water volume on hydrogen production becomes highly significant at higher amounts of catalyst, and in order to increase the volume of hydrogen gas at high levels of catalyst, the amount of water must also be increased. The $RuCl_3$ catalyst can be active on both the surface and in the interior of the biomass, contributing to the formation of more gaseous products and hydrogen, since it can be diffused into the interior of the biomass along with water via dissolution. The $RuCl_3$ catalyst is also efficiently dispersed in the interior of the biomass with water as more $RuCl_3$ is dissolved with an increasing volume of water at 250 °C. This provides a catalytic effect on both the surface and inside of the biomass leading to an increase in production of hydrogen other gas products.

The interaction effects of catalyst amount/reaction time and catalyst amount/biomass weight are also effective on hydrogen production. These effects can be evaluated from the 3D surface plots of hydrogen volume plotted against catalyst amount/reaction time and catalyst amount/biomass amount, which were shown in Figure 4 (a) and (b).

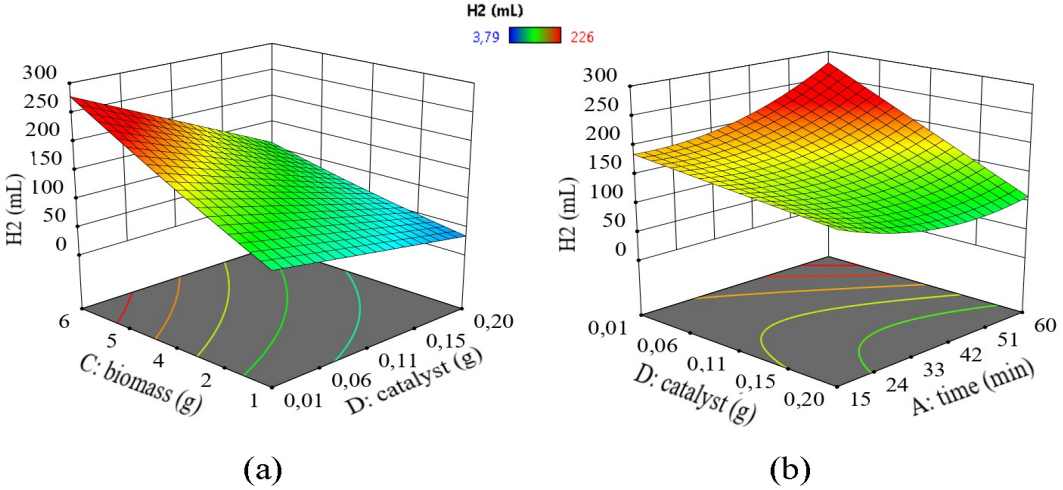

Figure 4. 3D response surface plots of hydrogen volume as function of (a) biomass amount (g)/catalyst amount (g); (b) catalyst amount(g)/time.

It can be seen from Figure 4 (a) that at higher levels of catalyst amounts (D+0.20g), it is possible to obtain more hydrogen gas at shorter reaction times, but the volumes of hydrogen gas obtained are not as high as the lower levels of catalyst amounts even if the reaction times are shortened. At low catalyst amount levels (D-0.01g), the reaction time is highly effective on the process and the need to be extended to increase the produced hydrogen volumes. Figure 4 (b) shows an increase in the effect of the amount of catalyst on the process by increasing the amount of biomass in the reactor and higher volumes of hydrogen can be produced with increasing the biomass feed of the reactor at lower levels of catalyst amount. This is due to the fact that longer reaction times are required to complete the interaction of a certain amount of dissolved catalyst with the biomass, due to the lower mass ratio of catalyst/biomass.

The ANOVA results showing the significance of the process parameters and on carbon dioxide production and R^2 values are given in Table 4. The values of R^2 and adjusted R^2 were calculated as 0.8858 and 0.7717. The Predicted R^2 of 0.5882 is in reasonable agreement with the adjusted R^2. These results indicated that the proposed equation was appropriate to evaluate the relationship of hydrogen volume with the input variables. The empirical model defining the relative impact of the input variables on carbon dioxide volume in terms of coded values is shown below;

Y3 ={183.1+2.3A – 17.6B+122.7C – 30.0D + 6.3AB – 11.5AC – 5.4AD + 2.9BC – 1.3BD – 44.9CD - 9.5A}2 +19.62 -2.5 C2 – 1.7 (Eq. 3)

where Y3 represents the carbon dioxide volume. According to ANOVA results, biomass amount (C) and catalyst amount (D) are the significant parameters which are effective on produced CO_2 volume. The value of the factor co-efficient of C, which is relatively higher than the others, indicates that biomass concentration is highly effective on carbon dioxide volume. The direction of the effect is positive which means the increasing levels of biomass concentration will increase the produced carbon dioxide volumes. Biomass concentration has no interaction with the other factors as the model terms AC, BC and CD were found to be insignificant. The other variable, which has a significant effect on carbon dioxide production, is the catalyst amount. The factor coefficient of “D” in equation is negative indicating that the higher levels of catalyst amount will result in a decrease in carbon dioxide production. The carbon dioxide volume as function of amount of catalyst and amount of biomass is given in Figure 5.

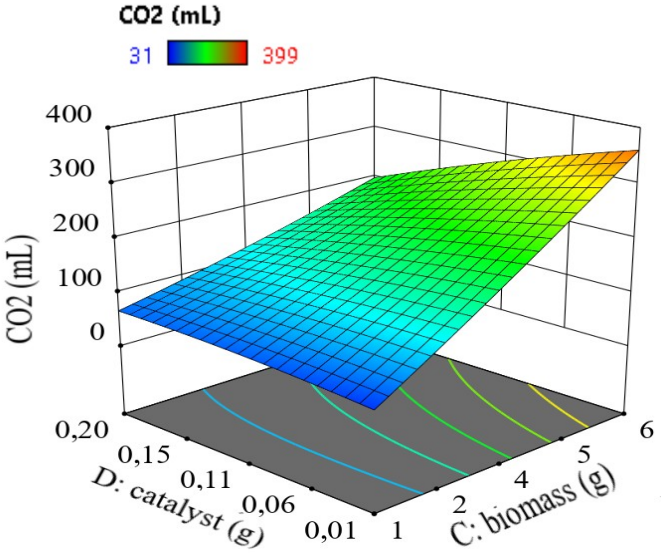

Figure 5. 3D response surface plots of carbon dioxide volume as function of catalyst amount (g)/ biomass amount (g).

Optimization of the process parameters for maximum hydrogen production

The main part of the study was to determine the optimum conditions for high hydrogen production from co–gasification of sorghum biomass and coal by supercritical water gasification under mild conditions. Desirability function and numerical optimization method were used to optimize the variables by targeting the maximum total gas and hydrogen volume. Figure 6 shows the desirability values at the end of the hydrogen volume maximization study, with the desirability value of 1.0 depending on the selected maximum total gas with a maximum hydrogen content goal for the variables. The optimum conditions for maximum hydrogen production were determined as residence time of 59.3 minutes, water volume of 10.5 mL with a catalyst amount of 0.02 g. The optimal parameter values were validated by experiments. The predicted and experimental values are given in Table 6. The 3D response surface plot of desirability as a function of coal percent and water volume is given in Figure 5.

The experimental results were close to those predicted. 985 mL total gas was produced including 253 mL H_2 (1.7 mmol H_2/g feedstock). Hydrogen selectivity is calculated from Eq. (4) as 36.9 %. The total feedstock conversion was found as 76.0 % (w/w). Feedstock conversion was calculated from Eq. (5).

$$Hydrogen\,selectivity = \frac{(moles\ of\ H_2)}{(total\ moles\ of\ H_2 + CO_2 + CO + CH_4)} \times 100 \quad \text{(Eq.4)}$$

$$Conversion = \left[Total\ material\ loaded\ into\ the\ reactor\ (daf) - char\right] \times 100 \quad \text{(Eq.5)}$$

The remaining liquid was also qualitatively analyzed by GCMS and was found to include mainly furfural (15.4 min) 2, 4-dimethylfuran (28.6 min), and phenol (24.9).

Table 6. The predicted and experimental values of optimized process parameters for maximum hydrogen production.

	Time (min)	Water volume (mL)	Biomass (g)	Catalyst (g)	Total gas (mL)	H_2 (mL)	CO_2 (mL)	CO (mL)	CH_4 (mL)	Desirability
Predicted	59.3	10.5	6.0	0.02	699	265	348	51	35	1
Experimental	59.0	10.5	6.0	0.02	685	253	335	51	46	

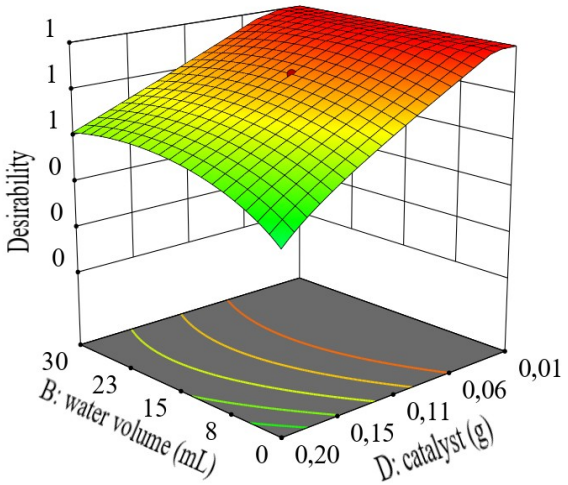

Figure 6. The 3D response surface plot of desirability function for maximum hydrogen volume against water volume (mL) and catalyst amount (g) at constant feedstock mass (6.0 g).

CONCLUSIONS

In this study, hydrothermal co–gasification of sorghum biomass is performed at a constant temperature of 250 °C in a batch type closed stainless-steel reactor. The individual and simultaneous effects of residence time (min), initial water volume (mL), feedstock amount (g) and catalyst amount on the responses of total gas volume, hydrogen yield and carbon dioxide production were evaluated by Box–Behnken design (BBD) combined with response surface modelling (RSM). The significance of the factors and their interactions were determined by Analysis of variance (ANOVA). It has been found that, in order to increase the total gas volume obtained from the process, the water volume should not be increased above a certain value. Also the reaction time can be shortened by increasing the amount of catalyst, or the reaction times should be kept longer if a high amount of gas is desired by using lower amounts of catalyst. The reaction time is to be kept low, the water volume must be reduced in order to achieve higher hydrogen yields. The effect of water volume on hydrogen production becomes highly significant at higher amounts of catalyst, and in order to increase the volume of hydrogen gas at high levels of catalyst, the amount of water must also be increased. The optimum conditions for maximum hydrogen production from 6.0 g of sorghum were determined as residence time of 59.3 minute, water volume of 10.5 mL with a catalyst amount of 0.02 g. At these conditions 76.0 % of biomass is converted to 685 mL total gas with 36.9% hydrogen selectivity.

ACKNOWLEDGEMENTS

This study was funded by Çukurova University Research Grant (Project numbers: FBA-2017-9823).

REFERENCES

1. Omer A M. Energy, environment and sustainable development. Renewable and sustainable energy reviews. 2008;12(9):2265-300

2. Dunn S. Hydrogen futures: Toward a sustainable energy system. Int J Hydrogen Energy. 2002;27(3):235-64.

3. Ni M, Leung DYC, Leung MKH, Sumathy K. An overview of hydrogen production from biomass. Fuel Process Technol. 2006; 87(5):461-72.

4. Alauddin ZABZ, Lahijani P, Mohammadi M, Mohamed AR. Gasification of lignocellulosic biomass in fluidized beds for renewable energy development: A review. Renewable and Sustainable Energy Reviews. 2010;14(9):2852-62.

5. Onwudili JA, Williams PT. Hydrothermal gasification and oxidation as effective flameless conversion technologies for organic wastes. J Energy Inst. 2008; 82(2)102-9.

6. Kruse A. Hydrothermal biomass gasification. Journal of Supercritical Fluids. 2009;47(3):391-99.

7. Elliott DC. Catalytic hydrothermal gasification of biomass. Biofuels, Bioproducts and Biorefining. 2008;2(3):254-65.

8. Azadi P, Farnood R. Review of heterogeneous catalysts for sub- and supercritical water gasification of biomass and wastes. International Journal of Hydrogen Energy. 2011;36(16):9529-41.

9. Osada M, Sato T, Watanabe M, Shirai M, Arai K. Catalytic gasification of wood biomass in subcritical and supercritical water. Combust Sci Technol. 2006;178(1–3):537–52.

10. Cortright RD, Davda RR, Dumesic JA. Hydrogen from catalytic reforming of biomass-derived hydrocarbons in liquid water. Nature. 2002;289-92.

11. Kruse A, Dahmen N. Hydrothermal biomass conversion: Quo vadis? J Supercrit Fluids. 2018;134:114-23.

12. Montgomery DC. Design and Analysis of Experiments Eighth Edition. 2012.

13. Box G, Draper N. Empirical Model Building and Response Surfaces, 1st Edition. Wiley Ser Probab Math statics, ISBN 978-0471810339. 1987.

14. Box GEP, Behnken DW. Some New Three Level Designs for the Study of Quantitative Variables. Technometrics. 1960.

15. Ferreira SLC, Bruns RE, Ferreira HS, Matos GD, David JM, Brandão GC, et al. Box-Behnken design: An alternative for the optimization of analytical methods. Analytica Chimica Acta. 2007;597(2):179-86.

16. Wu H, Hanna MA, Jones DD. Fluidized-bed gasification of dairy manure by Box-Behnken design. Waste Manag Res. 2012; 30(5):506-11.

17. Bazargan A, Bazargan M, McKay G. Optimization of rice husk pretreatment for energy production. Renew Energy. 2015; 77:512-20.

18. Inayat M, Sulaiman SA, Kurnia JC. Catalytic co-gasification of coconut shells and oil palm fronds blends in the presence of cement, dolomite, and limestone: Parametric optimization via Box Behnken Design. J Energy Inst. 2019;92(4):871-82.

19. Samiee-Zafarghandi R, Karimi-Sabet J, Abdoli MA, Karbassi A. Supercritical water gasification of microalga Chlorella PTCC 6010 for hydrogen production: Box-Behnken optimization and evaluating catalytic effect of MnO 2 /SiO 2 and NiO/SiO 2. Renew Energy. 2018; 126:189.

20. Hasanoğlu A,Demirci İ, Seçer A. Hydrogen production by gasification of Kenaf under subcritical liquid–vapor phase conditions. International Journal of Hydrogen Energy.2019;44(27):14127-36.

21. Hesenov A, Atanur OM, Erbatur O, Irmak S, Meryemoglu B. Aqueous-phase reforming of biomass using various types of supported precious metal and raney-nickel catalysts for hydrogen production. International Journal of Hydrogen Energy. 2010;35(22):12580-7.

22. Tükel S, Sahin PB, Yildirim D. Optimization of lipase-catalyzed synthesis of fructose stearate using response surface methodology. Artif Cells, Nanomedicine Biotechnol. 2013;41(5):344-51.

23. Stat-Ease, Inc. 2020. Design-Expert Software:Tutorials. Retrieved from: https://www.statease.com/docs/v12/tutorials/

24. Laudise RA. Chemical & Engineering News Archive. 1987;65(39):30-43

25. Sasaki M, Adschiri T, Arai K. Production of cellulose II from native cellulose by near-and supercritical water solubilization. Journal of agricultural and food chemistry. 2003;51(18): 5376-81.

JOTCS B
Journal of the Turkish Chemical Society
Section: B
Chemical Engineering
TURKISH CHEMICAL SOCIETY

Ultimate Eradication of Acid Orange 7 from Contaminated Liquid via Synthesized Mesoporous Goethite

Davoud Balarak[1], Fatemeh Ganji[2], Periakaruppan Rajiv[3], Chinenye Adaobi Igwegbe[4]*, Joshua O. Ighalo[4,5]

[1]Department of Environmental Health, Health Promotion Research Center, Zahedan, University of Medical Sciences, Zahedan, Iran.
[2]Student Research Committee, Zahedan University of Medical Sciences, Zahedan, Iran.
[3]Department of Biotechnology, Karpagam Academy of Higher Education, Eachanari Post, Coimbatore 641 021, Tamil Nadu, India.
[4]Department of Chemical Engineering, Nnamdi Azikiwe University, P.M.B. 5025, Awka, Nigeria.
[5]Department of Chemical Engineering, University of Ilorin, P. M. B. 1515, Ilorin, Nigeria.

Abstract: This paper carried out the study on the adsorption of Acid Orange 7 (ACO7) from aqueous solutions by mesoporous goethite (MPG). The adsorbent was characterized by XRD, FE-SEM, BJH desorption, and BET. The effect of process variables such as MPG dosage, reaction time, concentration of ACO7, pH, and reaction temperature on the ACO7 uptake capacity were systematically investigated in an attempt to illustrate adsorption performance of MPG. Optimal condition for the adsorption process was 1 g/L adsorbent dosage, temperature of 328 K, pH of 3, 75 minutes' contact time and 100 mg/L ACO7 concentration which yielded a removal efficiency of 90.13%. The adsorption kinetic was best fit to the intra-particle diffusion model while the equilibrium isotherm was best fit to the Langmuir model, suggesting that homogeneous uptake was the principal mechanism adopted in the process of ACO7 adsorption with a monolayer adsorption capacity, q_m of 117.9 mg/g. The study revealed that the pseudo-second order model and the Langmuir isotherm model were the best-fit kinetics and isotherm models to describe the process. The uptake of ACO7 by MPG was endothermic and spontaneous. The major mechanisms for ACO7 uptake onto MPG were pore diffusion, hydrogen bonds, π – π stacking interactions and hydrophobic interactions. MPG has excellent reusability potential with only an 8% drop in performance after 8 cycles. These results indicate that MPG has wide application prospects in removing ACO7 from wastewater.

Keywords: Acid Orange 7, Adsorption, Dye, Goethite, Water Pollution

Submitted: January 23, 2021. **Accepted:** March 01, 2021.

Cite this: Balarak D, Ganji F, Rajiv P, Igwegbe CA, Ighalo JO. Ultimate Eradication of Acid Orange 7 from Contaminated Liquid via Synthesized Mesoporous Goethite. JOTCSB. 2021;4(1):13–26.

***Corresponding author. Email:** ca.igwegbe@unizik.edu.ng

INTRODUCTION

Dyes are used all over the world for miscellaneous purposes (1, 2). Colorizing the industrial products of textile, paper, printing leather, food and cosmetic produce large amounts of colored wastewater (3-5). Pulp, paper, and textile industries have been considered as major polluting units across the world (6-8).

Industrial dyes are the main sources of environmental pollution due to their high-toxicity, non-biodegradability, mutagenic, and carcinogenic characteristics (9, 10). Effluent containing dyes should be treated before it is discharged to the environment due to its toxicity (11, 12). Hence, there is an immense interest in the uptake of dyes from polluted water using non-toxic, cost-effective and biodegradable materials (13, 14). Acid Orange 7 (2-naphthol orange or Orange II) is an inexpensive and moderately fast azo dye (15, 16). Its popular use and regular occurrence in effluents (17) was the reason it was selected for the current study.

With the increasing public concerns on environmental protection, removal of colorful

dyestuffs from wastewater has become an especially important issue (18, 19). Dye removal can be managed via coagulation, biodegradation, chemical degradation, and photo-degradation and adsorption methods (20). Every method has advantageous and disadvantageous from the points of effectiveness and cost except adsorption (20, 21). In recent years, adsorption method with low cost, high operability and no secondary pollution has been widely used to remove dyes in aqueous environments and soils (12, 21). There are a lot of investigations about the utilization of renewable and low budget adsorbents like *Azolla filiculides*, *Lemna minor*, Canola, pumice stone, bentonite, cherry kernels, husk rice, sewage sludge and montmorillonite (22-24).

Goethite is an environmental stable iron oxy-hydroxide (25). Researchers have employed it for water management (26, 27). The study on the capacity of adsorption of goethite is scarce (28, 29). The utilization of mesoporous goethite (MPG) for the adsorptive uptake of pollutant dye like Acid Orange 7 (ACO7) is unreported, therefore, this study was done. The adsorption capacity of MPG for ACO7 uptake from liquid was examined. The characterization of MPG was done via the X-Ray Diffraction (XRD), Field Emission Scanning Electron. Microscopy (FE-SEM), Barrett-Joyner-Halenda (BJH) desorption and Brunauer-Emmett-Teller (BET). The effects of several process elements such as MPG dose, pH, time of contact, ACO7 concentration, and temperature on adsorbate uptake was examined. This study also considered the adsorption kinetics, isotherms, thermodynamics and mechanism of the adsorption process.

EXPERIMENTAL SECTION

Reagents

Acid Orange 7 (2-naphthol orange or Orange II) is an azo dye (molecular formula:$C_{16}H_{11}N_2NaO_4S$, molecular mass:350.32g/mol). The molecular structure of the ACO7 has been represented in Figure 1. Ferrous sulfate heptahydrate, Acid Orange 7, hydrogen peroxide (30%), sodium hydroxide, and hydrochloric acid were obtained from Sigma Aldrich. A stock solution of ACO7 (500 mg/L) was synthesized through suspending a suitable measurement of the ACO7 in ultrapure-water. All reagents used in the study were of analytical grade.

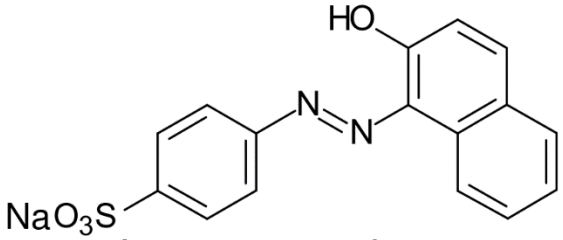

Figure 1: Structure of ACO7.

MPG preparation

The MPG was synthesized using the procedure reported by (**See supplementary**). The characterization of MPG was done via the XRD, FE-SEM, BJH desorption and BET.

Batch adsorption studies

The effect of process factors such as MPG dose, time of contact, initial ACO7 concentration, pH and temperature was considered during a batch process. The temperature of the batch adsorption experiment was varied at 10, 25, 40 and 55 °C; and the removal of ACO7 was performed as described above. The effect of contact time was evaluated through measurements 10, 20, 30, 45, 60, 90 and 120 min. Each experiment was done using a 100 mL solution of the dye having a specified initial concentration. The pH of the dye solution was adjusted using 0.1 N HCl or NaOH. A known quantity of MPG was introduced into the ACO7 solution and magnetically stirred at 160 rpm for a given period. When the contact time is achieved, the solution is filtered out by Whatman filter paper. Dye concentrations were analyzed using UV/VIS spectrophotometry (Shimadzu, Japan; Model DR 5000) at λ_{max} = 484 nm. The ACO7 adsorbed on MPG was evaluated using Eq. 1 (30):

$$q_e = \frac{(C_0 - C_e)V}{m} \quad \text{Eq. 1}$$

Where C_0 (mg/L) is the initial ACO7 concentration, *Ce* (mg/L) is the ACO7 concentration at a specific time, V (m^3) is the volume of ACO7 solution, and M (g) is the MPG amount, respectively.

The % removal efficiency is determined using Eq. 2 (31). The dimensionless separation factors (R_L) is determined using Eq. 3 (32), where K_L is the Langmuir constant.

$$R_e(\%) = \frac{(C_0 - C_e)}{C_0} \times 100 \quad \text{Eq. 2}$$

$$R_L = \frac{1}{1 + K_L C_0} \quad \text{Eq. 3}$$

RESULTS AND DISCUSSION

Characterization of MPG

XRD analysis was done through an X-ray diffractometer with Philips PNA-analytical diffractometer. Figures 2-3 shows the characterization of MPG. The MPG reveals typical characteristic peaks (Figure 2) at 19.44°, 33.09°, 36.75°, 44.64°, 59.71° and 66.97°, corresponding to 110, 130, 111, 140, 151 and 061 of MPG (JCPDS no. 29-0713), respectively. The sharp and intense MPG peaks suggest that the material is crystalline in nature (33). FE-SEM experiment was carried out using a scanning electron microscopy (SEM) (JEOL, JSM 6500F). FE-SEM image shown in Figure 3 reveals the presence of spherical clusters, but most agglomerated. The heterogeneous outlook suggests the MPG have good surface area and applicable as a

sorbent (34). The N_2 adsorption isotherm was obtained by means of Quantachrom ChemBET-3000 USA. N_2 adsorption-desorption isotherms and BJH desorption of goethite and MPG is shown in Figure 4. The adsorption-desorption isotherm curves of MPG exhibit a type IV isotherm with H3 hysteresis loop which reveals that the adsorbent has a mesoporous nature. However, the adsorption-desorption isotherm curves of goethite reveal a type III isotherm and the hysteresis loop becomes inconspicuous, indicating no typical pores appearance (29). The specific surface area of MPG and common goethite are 194.35 and 149.64 m^2/g, respectively. It can be observed that the synthesized MPG has a greater surface area than goethite. Specific surface area is an important property of an adsorbent as it affects the sorbate-sorbent interface and influences the extent of adsorbate uptake (35).

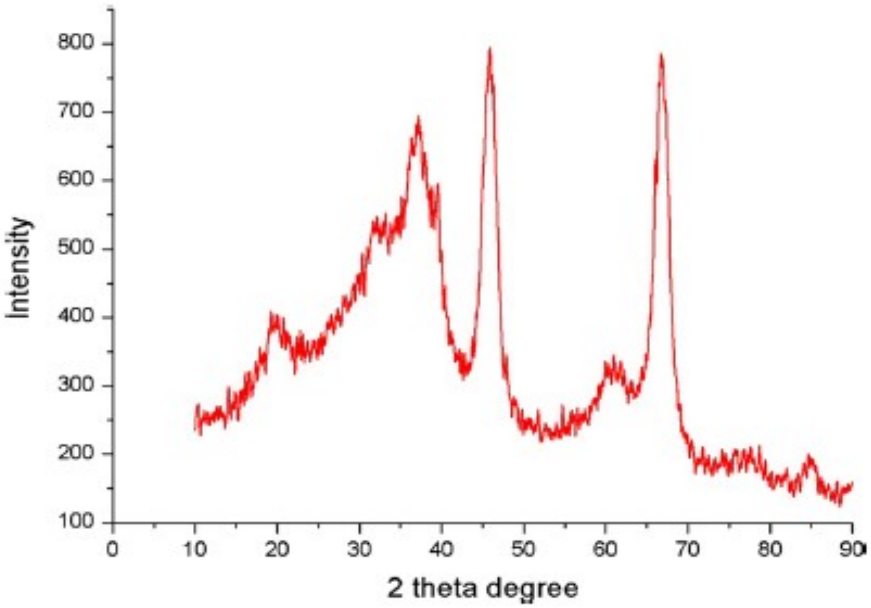

Figure 2: The XRD of MPG.

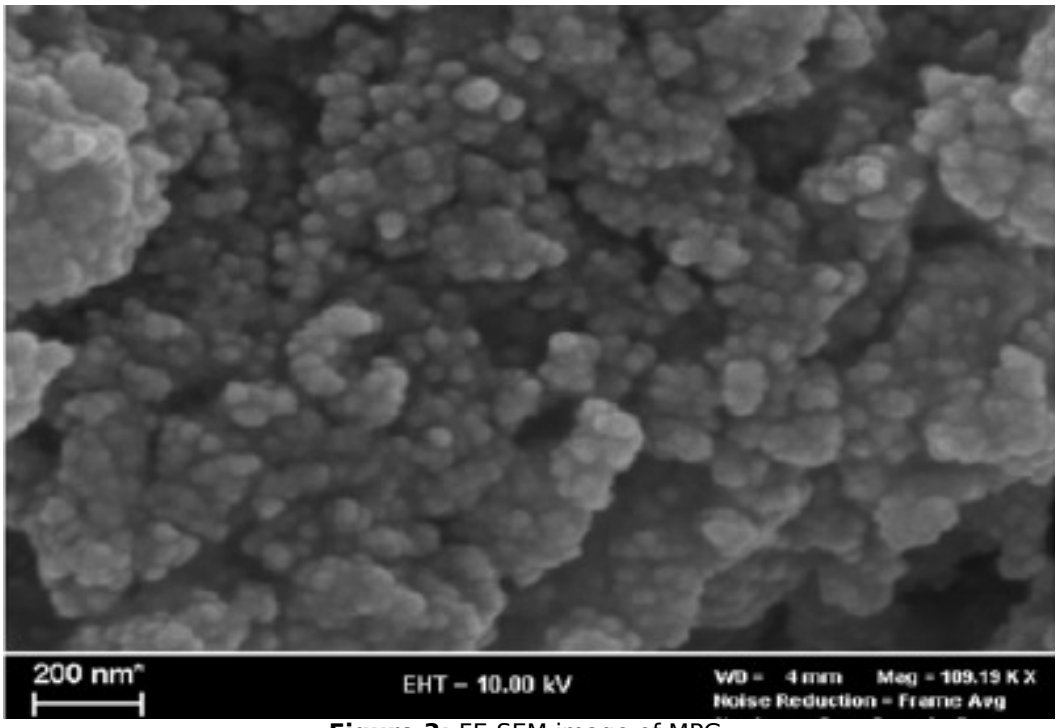

Figure 3: FE-SEM image of MPG.

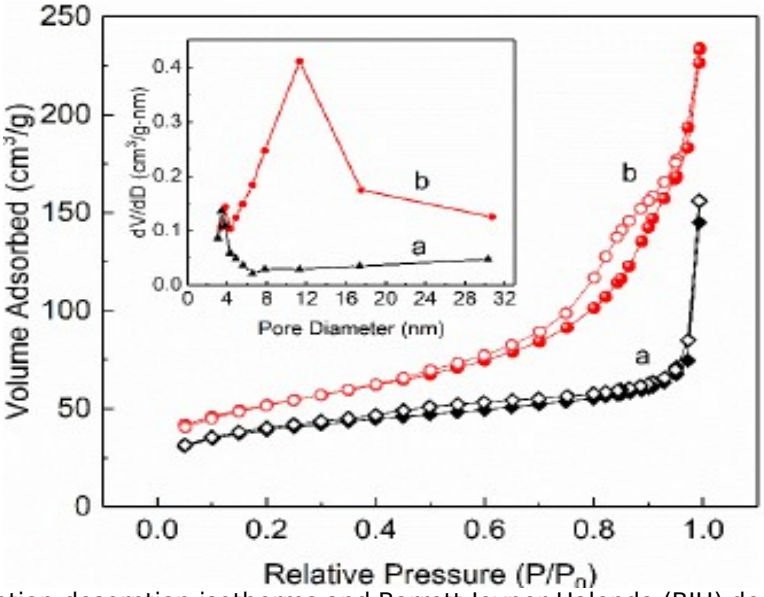

Figure 4: N_2 adsorption-desorption isotherms and Barrett-Joyner-Halenda (BJH) desorption of goethite (a) MPG (b).

Effect of process factors

Impact of pH

The impact of pH on ACO7 removal was inspected at a contact time of 75 min, MPG dose of 1 g/L, initial ACO7 concentration of 100 mg/L and at 25± 2 °C. The pH was studied between 3–11. As shown in Figure 5, the amount of ACO7 removal decreased from 90.88 to 48.45%, when pH changed from 3.0 to 11.0. In contrast, at a higher pH, the aggregation of the zwitterionic form of ACO7 molecules occurs leading to electrostatic interactions between the carboxyl groups on the MPG (36). This aggregation of ACO7 leads to the formation of large ACO7 dimers that are then unable to penetrate the MPG, decreasing the adsorptive removal of ACO7 (37). In acidic pH values, the adsorbent surface has a net positive charge, and a complexation occurs between the positive charges of adsorbent and the negative ions of the dye (36). It demonstrates the ability to compete between -OH ions in dye with available and active sites at the adsorbent surface (26). The optimum pH was at 3 and this was utilized for other experiments.

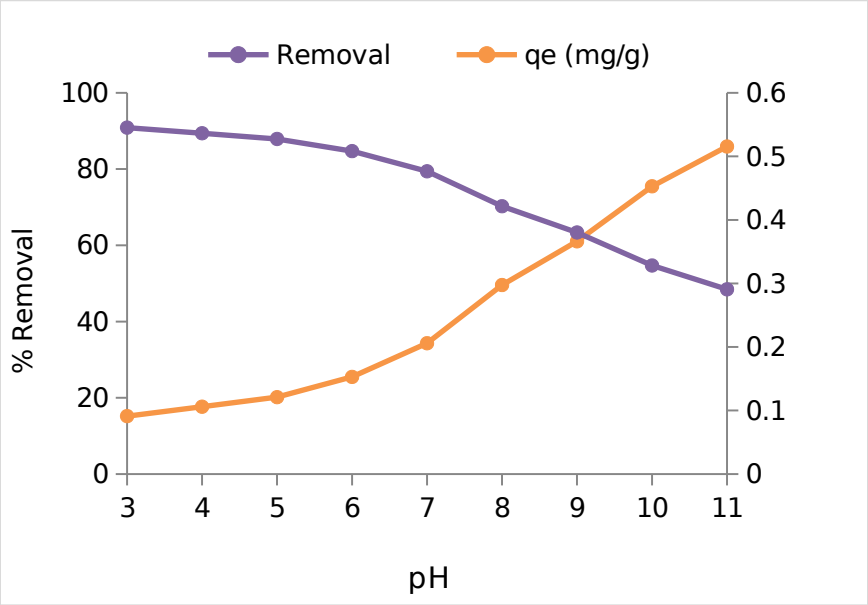

Figure 5: Impact of pH on ACO7 removal (at time =75 min, MPG dose = 1 g/L, C_0 = 100 mg/L, temp = 25 °C).

MPG dose effect

The effect of MPG dose on ACO7 removal was investigated at 25± 2 °C. As shown in Figure 6, the effect of dosage on MPG adsorbed ACO7 was studied with doses of the range 0.2 - 1.4 g/L. The adsorption ratio increased rapidly as MPG dose

increased and the adsorption ratio was not increased considerably when MPG doses were higher than 0.6 g/L. When the dosage of MPG was about 1 g/L, the adsorption ratio of ACO7 reached the maximum (90.88%). Increasing the dosage of MPG, the adsorption sites of adsorbent could not be full-scaled used and made some adsorption sites approached so that the adsorption capacity of the ACO7 per unit of MPG gradually reduced (38). In general, the dosage of MPG affects the surface area and the available active sites (39). The optimal MPG dosage was 1 g/L and this was used for the rest of the experiments.

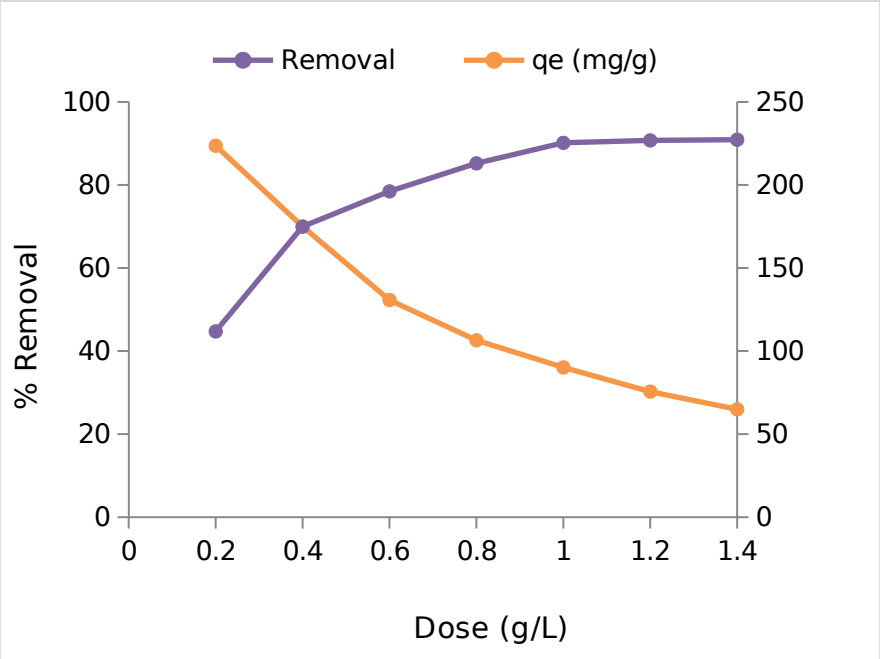

Figure 6: Effect of MPG mass on ACO7 adsorption (at C_0 = 100 mg/L, temp = 25 °C, time = 75 min, pH = 3).

Impact of temperature

The investigation of temperature effect on the uptake of ACO7 was done by measurements at 10, 25, 40 and 55 °C (Figure 7). The results showed that ACO7 uptake on MPG was improved with elevating temperature. With increasing temperature, the mobility of dye molecules increases, which can facilitate penetration to surface/interface of adsorbent (40-41). This showed that the process was endothermic which was also confirmed by the thermodynamics modeling results, and the increasing temperature was beneficial to the adsorption of ACO7 on MPG. The result was similar to those reported by some researchers (33, 42). Another hypothesis was that as the temperature increases, the approached sites, structure and volume of the pores on the surface of the adsorbent were increased, which enhanced the relevant adsorption properties of the MPG adsorbents (43).

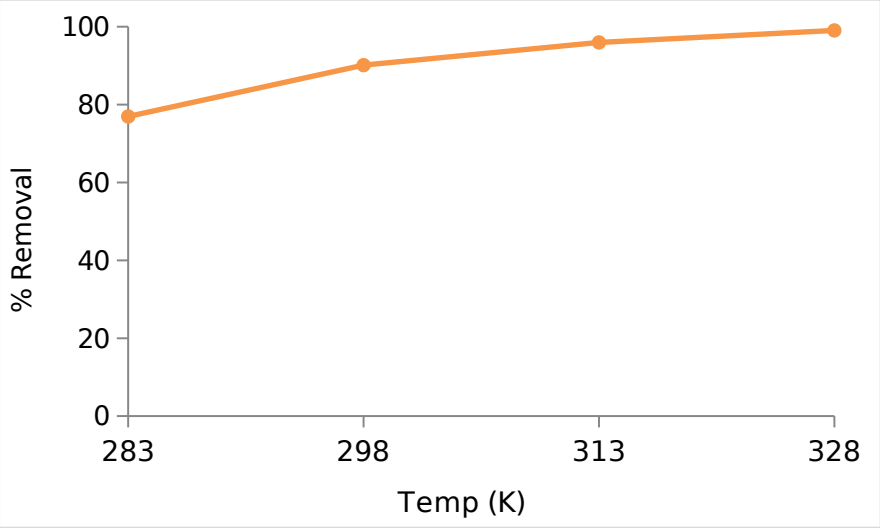

Figure 7: Impact of adsorption temperature on ACO7 removal (at C_0 = 100 mg/L, MPG dose = 1 g/L, time = 75 min, pH = 3).

Impact of ACO7 concentration and contact time

The adsorptive uptake was rapidly increasing at the commencement of the adsorption process and gradually reduced as the adsorption progressed towards equilibrium (Figure 8). This was because the amount of the dyes in the solution was high at the start of experiments, and there were still much-unoccupied adsorption sites of MPG (44). High initial concentration also favored the adsorptive uptake of ACO7 because it leads to a greater mass transfer driving force of the adsorbate across the sorbate-sorbent liquid film (45, 46). Equilibrium was achieved after about 75 minutes. As the adsorption proceeding, the decreasing adsorption rate gradually decreased due to the adsorption sites were gradually occupied by contaminants (47).

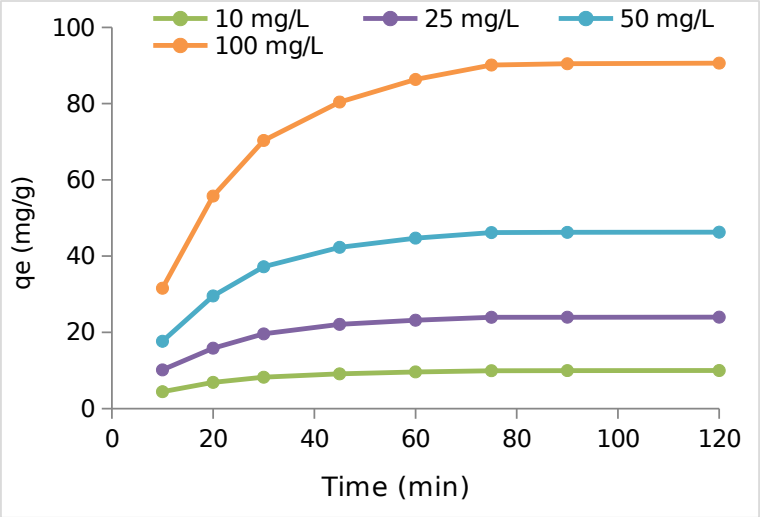

Figure 8: Effect of ACO7 concentration and time on ACO7 uptake (at MPG dosage = 1 g/L, pH = 3.0, temp = 25 °C).

Adsorption isotherm modeling

The adsorption of ACO7 onto MPG was modeled using the Langmuir (48), Freundlich (49), Temkin (50) and Dubinin–Radushkevich (D-R) (51) isotherms. From Table 1, the Langmuir isotherm model was observed to be best-fit for the adsorption data based on the closeness of the R^2 values to 1. The values of the separation factor (K_L) showed an increasing trend with temperature increase. This suggests that ACO7 adsorption is an endothermic process and this is confirmed by the thermodynamics result. Since the K_L values are less than 1, it also shows that the adsorption process is favorable. The good adaptability of Langmuir isotherm to experimental data means that homogeneous surface exists in MPG and that the adsorption of ACO7 onto MPG takes place as a monolayer (52). The monolayer adsorption capacity of ACO7 onto MPG is 117.9 mg/g (at 328 K).

The K_F values of the Freundlich isotherm was in the range of 4.72~9.14 and it showed an increasing trend with temperature increase, again confirming the endothermic nature of ACO7 uptake by MPG. The values of 1/n were also found in the range of 0.141~0.279 at all temperatures used, signifying again that adsorption is favorable. The Temkin isotherm model parameters K_T and B_T increased with temperature which indicates that the heat of adsorption of ACO7 onto the surface of MPG is endothermic. From the D-R isotherm, the values of E were found all smaller than 16 kJ/mol (Table 1), suggesting that the sorption type of ACO7 onto MPG was majorly by physical mechanisms.

Table 1: Isotherm parameters for adsorption of ACO7 onto MPG at various temperatures.

Temp (K)	Freundlich			Langmuir			
	K_F	1/n	R^2	q_m	R_L	K_L	R^2
283	4.721	0.141	0.814	90.62	0.441	0.0127	0.992
298	6.194	0.185	0.849	97.25	0.337	0.0196	0.995
313	7.962	0.224	0.879	106.4	0.281	0.0256	0.998
328	9.147	0.279	0.825	117.9	0.226	0.0342	0.991
Temp (K)	**Temkin**			**D-R**			
	B	K_T	R^2	q_s	**E**		R^2
283	7.42	0.112	0.918	45.69	0.425		0.904
298	8.73	0.195	0.895	51.25	0.691		0.925
313	9.13	0.264	0.927	56.74	0.819		0.896
328	9.87	0.371	0.943	63.79	1.054		0.941

Kinetics modeling

The kinetics of the adsorption of ACO7 onto MPG was modeled by the pseudo-first order (53), pseudo-second order (54) and intra-particle diffusion (55) models. The results are summarized in Table 2. From the table, it can be observed that the intra-particle diffusion model is the best fit for describing the adsorption process due to its high coefficient of determination (R^2) values. The intra-particle diffusion model proceeds in two steps hence the results shown in Table 2 are for step 1 and 2. In the first step, the uptake of ACO7 occurred on the surface of adsorbents, while in the second step, the adsorbate penetrates through the pores of the adsorbents (56). The values of K_1, and K_2 are the rate parameters for the first step and second step respectively. The R2 vales of the IPD step is higher which suggests that the adsorption takes place majorly on the surface. From modeling itself, it was observed that the intercept was not equal to zero, this explained that intra-particle diffusion was not the only rate-controlling step in the adsorption process. The pseudo-second order model was also well fitted to the adsorption data with similar conclusions obtained by previous research (57, 58). This is suggestive that both the amount of available MPG active sites and the concentration of ACO7 adsorbate in the aqueous phase affects the adsorption process (59).

Thermodynamics modeling

Thermodynamics modeling was done to determine the value of some of the parameters, like the change in enthalpy (ΔH°), Gibbs energy (ΔG°) and entropy (ΔS°) for the adsorption of ACO7 on MPG were calculated at different temperatures using Eq. 4-5 (10)

$$\Delta G° = - RT \ln K \quad \text{Eq. 4}$$

$$\ln K = \frac{\Delta S^0}{R} - \frac{\Delta H^0}{RT} \quad \text{Eq. 5}$$

The values of ΔH°, ΔG° and ΔS° parameters obtained from the modeling are summarized in Table 3. The negative values of ΔG° suggest ACO7 uptake by MPG is spontaneous and the greater the negative value of ΔG° goes, the more energetically favorable the adsorption becomes (60). The enthalpy change (ΔH°) was +57.58 KJ/mol, therefore, ACO7 uptake by MPG is an endothermic process (43). Also, the positive value of entropy change (ΔS°= +0.212 KJ/mol·K) indicates that the randomness of the solid-solution interface increases during the adsorption of the ACO7 to the MPG (61, 62). The small magnitude of the values of ΔG° (<20 KJ/mol) suggest that the uptake of ACO7 onto MPG is by a physical mechanism (63).

Adsorption mechanism

To gain a proper understanding of the nature of the adsorption process, it is important to conduct a holistic mechanistic analysis (35). Based on the isotherm and thermodynamics modeling studies, it is surmised that physical interactions are the major uptake mechanism of ACO7 onto MPG. At optimal pH (3.0), there is complexation between Fe cations on the MPG surface and the ACO7 adsorbate. These coordination surface complexes are formed by coordinate covalent interactions between the ligands (ACO7 in this case) and the metallic ions (Fe cations). This is achievable because ACO7 has acid dissociation constants of 11.4 (pK_{a1}) and 1.0 (pK_{a2}) (64) hence has valence electrons at the optimum pH (3.0).

However, since physical interaction forces are more significant at these optimum conditions, the presence of Van der Waals' forces are also responsible for much of the uptake (65). This is due to hydrogen bonds between –OH on goethite and the hydrogen atoms on the adsorbent. Furthermore, at the zwitterionic form of the adsorbent, the solubility is usually low and the hydrophobic effect of the surrounding aqueous phase increases the adsorptive uptake as the ACO7 then possesses a greater affinity for the solid phase (MPG in this case).

Based on the kinetic modeling, it is also observed that pore diffusion is another important mechanism of ACO7 uptake onto MPG. From Figure 1, the multiple benzene rings in ACO7 shows it is a polycyclic aromatic compound. These benzene rings possess electron-rich zones around the carbon atoms that could induce a stacking effect on the adsorbent. Such π – π stacking interactions are an important mechanism of uptake for the adsorption process. The different mechanisms for ACO7 uptake onto MPG are surface complexation, hydrogen bonds, pore diffusion, hydrophobic interactions, and π – π stacking interactions and these are summarized in Figure 9.

Comparison with other adsorbents

In this section, the adsorption capacity of other adsorbents for ACO7 uptake was compared with that of MPG. The findings are summarized in Table 4 to four significant figures and sorted in decreasing order. It was also important to report the pH and temperature at which these were achieved because they are relevant factors that affect the adsorption process. It can be observed that MPG have intermediate adsorption capacity in comparison with other adsorbents reported in literature. It is also observed that for most adsorbents, a low pH is required for the effective performance of the adsorbent. The implication in sustainable water management is in pre-acidification of effluent before adsorptive treatment.

Table 2: Summary of kinetics modelling for ACO7 onto MPG

C_o (mg/L)	q_e exp (mg/g)	PFO			PSO			IPD (step 1)			IPD (step 2)		
		K_1	q_e	R^2	K_2	I	R^2	K_1	q_e	R^2	K_2	I	R^2
10	9.71	0.073	3.72	0.841	0.051	1.951	0.859	0.721	0.211	0.956	0.051	1.951	0.859
25	23.67	0.059	9.14	0.872	0.098	2.762	0.872	0.941	0.495	0.942	0.098	2.762	0.872
50	46.28	0.061	23.73	0.804	1.091	4.826	0.884	1.452	0.652	0.935	1.091	4.826	0.884
100	90.62	0.043	45.84	0.897	1.273	5.839	0.865	1.872	0.841	0.948	1.273	5.839	0.865

PFO – Pseudo-first order, PSO – Pseudo-second order, IPD – Intra-particle diffusion

Table 3: Values of thermodynamic parameters for the adsorption of ACO7 onto MPG.

Temp (K)	ΔG^0 (KJ/mol)	ΔH^0 (KJ/mol)	ΔS^0 (KJ/mol K)
283	-2.83		
298	-5.47	57.58	0.212
313	-8.24		
328	-12.64		

Table 4: Comparison of sorbent performance for ACO7 uptake

Adsorbents	Temp (K)	pH	q_m (mg/g)	Ref.
AC from spent coffee/calcium-alginate beads	303	3.0	665.9	(64)
Mg-Al layered double hydroxide	298	-	485.6	(66)
Amberlite FPA-98	303	7.0	200.0	(15)
MPG	**328**	**3.0**	**117.9**	**This study**
MWCNT	298	7.0	47.72	(67)
Kenya tea pulps ash	-	2.0	41.66	(68)
ZnO nanoparticles	298	3.0	32.13	(69)
Spent brewery grains	303	4.5	30.50	(70)
Surfactant-modified zeolite	298	6.85	15.68	(71)
Zeolite-AC macro-composite	298	7.0	0.190	(72)

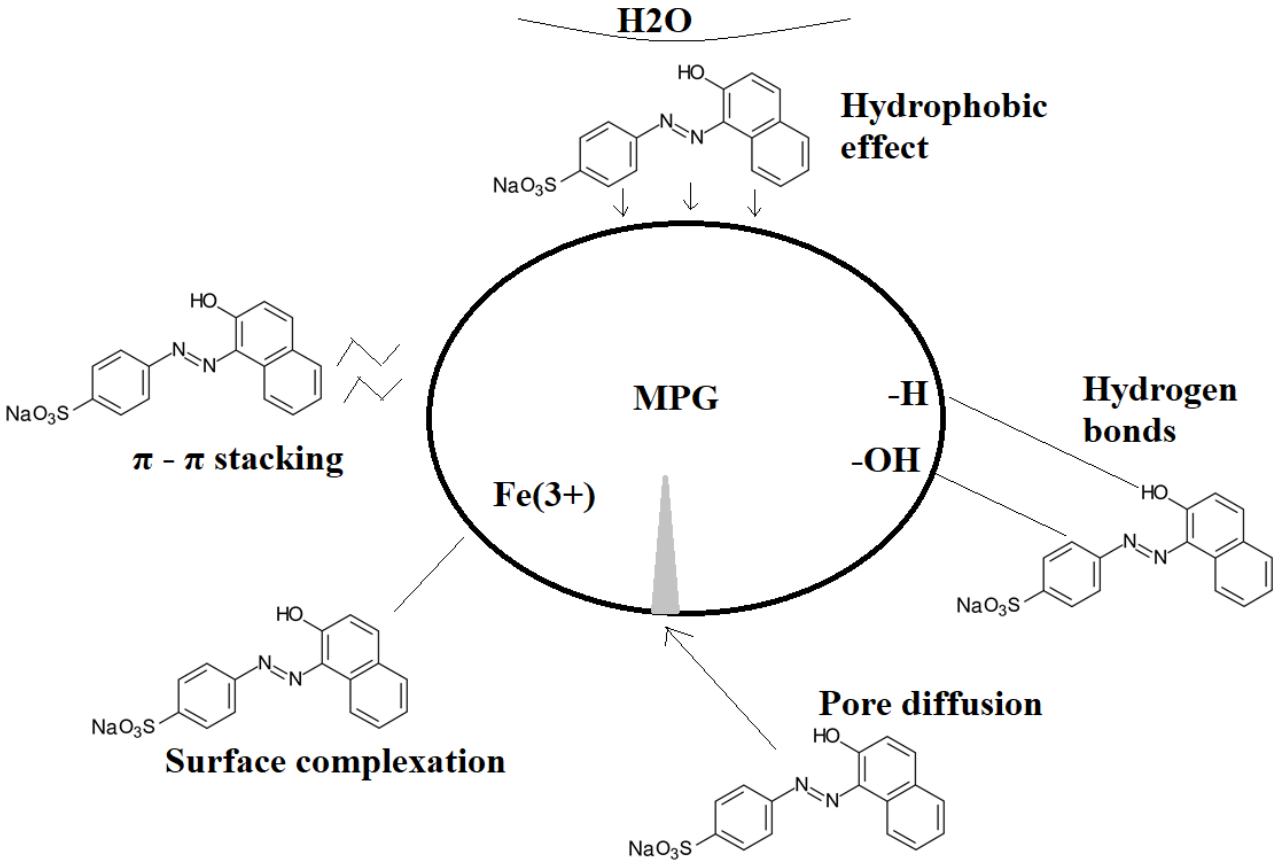

Figure 9: Summary of possible ACO7 adsorption.

Reuse Performance of MPG

The used MPG was regenerated as described by Erdem *et al.* (37) (*see Supplementary*). The ACO7 uptake capacity by the regenerated MPG for 8 cycles was shown in Figure 10. It can be observed that the ACO7 uptake capacity decreases moderately with the increase of cycle times from 90.13 mg/g for the fresh MPG to 83.17 mg/g for the 8 cycles. Therefore, these results still show that there was no clear deterioration observed for the regenerated MPG. It can be surmised that the MPG has excellent reusability potential with only an 8% drop in performance after 8 cycles. The ease of desorption and reuse could be due to the physical nature of interaction between the adsorbent and the adsorbate (73). Physical adsorption forces are not as strong as chemical bonds and are easily broken by the eluents (74).

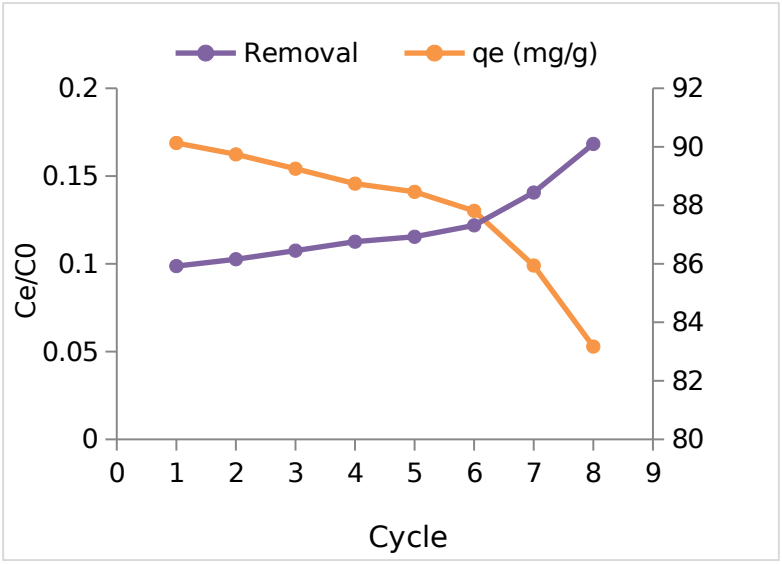

Figure 10: Comparison of ACO7 uptake capacity by fresh and regenerated MPG.

CONCLUSION

The adsorption of ACO7 by mesoporous goethite (MPG) was investigated. The BET specific surface area of MPG was 194.35 m^2/g. The adsorbent was heterogeneous, porous and crystalline in nature. Optimal condition for the adsorption process was 1 g/L adsorbent dosage, temperature of 328 K, pH of 3, 75 minutes' contact time and ACO7 concentration: 100 mg/L which yielded a removal efficiency of 90.13%. The uptake increased with increasing temperature and decreasing pH. The study revealed that intra-particle diffusion and Langmuir model were the best-fit kinetics and isotherm models to describe the process. The uptake of ACO7 by MPG was an endothermic and spontaneous process. The monolayer adsorption capacity of ACO7 onto MPG is 117.9 mg/g (at 328 K). Upon comparison with other adsorbents for ACO7 uptake, MPG has displayed an intermediate adsorption capacity. The major mechanisms for ACO7 uptake onto MPG were pore diffusion, hydrophobic, hydrogen bonds, π – π stacking, and interactions. MPG has excellent reusability potential with only an 8% drop in performance after 8 cycles. For future work, it will be interesting to investigate the mechanistic modeling via statistical physics techniques. The investigation could also be explored in column set-up to know its performance in industrial application scenarios.

REFERENCES

1. Arami M, Yousefi N, Mahmoodi NM. Evaluation of the adsorption kinetics and equilibrium for the potential removal of acid dyes using a biosorbent. Chem Eng J. 2008;139:2-10.

2. Moussavi GR, Mahmoudi M. Removal of azo and anthraquinone reactive dyes from industrial wastewaters using MgO nanoparticles. J Hazard Mater. 2009;168:806–12.

3. Balarak D, Zafariyan M, Igwegbe CA, Onyechi KK and Ighalo JO. Adsorption of Acid Blue 92 Dye from Aqueous Solutions by Single-Walled Carbon Nanotubes: Isothermal, Kinetic, and Thermodynamic Studies. Environmental Processes. 2021: 1-20.

4. Muthukumaran C, Sivakumar VM, Thirumarimurugan M. Adsorption isotherms and kinetic studies of crystal violet dye removal from aqueous solution using surfactant modified magnetic nanoadsorbent. Journal of the Taiwan Institute of Chemical Engineers. 2016;63:354-62.

5. Igwegbe CA, Mohmmadi L, Ahmadi S, Rahdar A, Khadkhodaiy D, Dehghani R, Rahdar S. Modeling of adsorption of Methylene blue dye on Ho-CaWO4 nanoparticles using Response surface methodology (RSM) and Artificial neural network (ANN) techniques. MethodsX. 2019;6:1779-97.

6. Eren E, Cubuk O, Ciftci H, Eren B, Caglar B. Adsorption of basic dye from aqueous solutions by modified sepiolite: equilibrium, kinetics and thermodynamics study. Desalination. 2010;252(1-3):88-96.

7. Özcan A, Özcan AS. Adsorption of Acid Red 57 from aqueous solutions onto surfactant-modified sepiolite. Journal of Hazardous Materials. 2005;125(1-3):252-9.

8. Ahmadi S, Mohammadi L, Rahdar A, Rahdar S, Dehghani R, Igwegbe CA, Kyzas GZ. Acid Dye Removal from Aqueous Solution by Using Neodymium (III) Oxide Nanoadsorbents. Nanomaterials. 2020;10(3):556.

9. Uddin MT, Rukanuzzaman M, Khan MMR, Islam MA. Adsorption of methylene blue from aqueous solution by jackfruit (Artocarpus heteropyllus) leaf powder: A fixed-bed column study. Journal of environmental management. 2009;90(11):3443-50.

10. Hevira L, Zilfa, Rahmayeni, Ighalo JO, Zein R. Biosorption of Indigo Carmine from Aqueous Solution by Terminalia Catappa Shell. Journal of Environmental Chemical Engineering. 2020;8(5):104290.

11. Ighalo JO, Adeniyi AG, Oke EO, Adewiye LT, Motolani FO. Evaluation of Luffa Cylindrica Fibers in A Biomass Packed Bed for The Treatment of Paint Industry Effluent Before Environmental Release. European Journal of Sustainable Development Research. 2020;4(4).

12. Pavan FA, Lima EC, Dias SL, Mazzocato AC. Methylene blue biosorption from aqueous solutions by yellow passion fruit waste. Journal of hazardous materials. 2008;150(3):703-12.

13. Assadi A, Soudavari A, Mohammadian M. Comparison of electrocoagulation and chemical coagulation processes in removing reactive red 196 from aqueous solution. Journal of Human, Environment and Health Promotion. 2016;1(3):172-82.

14. Deniz F, Karaman S. Removal of Basic Red 46 dye from aqueous solution by pine tree leaves. Chemical Engineering Journal. 2011;170(1):67-74.

15. Akazdam S, Chafi M, Yassine W, Gourich B. Removal of acid orange 7 dye from aqueous solution using the exchange resin amberlite FPA-98 as an efficient adsorbent: kinetics, isotherms, and thermodynamics study. Journal of Materials and Environmental Sciences. 2017;8(8):2993-3012.

16. Tatarchuk T, Paliychuk N, Bitra RB, Shyichuk A, Naushad M, Mironyuk I, et al. Adsorptive removal of toxic Methylene Blue and Acid Orange 7 dyes from aqueous medium using cobalt-zinc ferrite

nanoadsorbents. Desalin Water Treat. 2019;150:374-85.

17. Thirunavukkarasu A, Nithya R. Adsorption of acid orange 7 using green synthesized CaO/CeO2 composite: An insight into kinetics, equilibrium, thermodynamics, mass transfer and statistical models. Journal of the Taiwan Institute of Chemical Engineers. 2020.

18. Yousuf M, Mollah A, Gomes J, Das KK, Cocke DL. Electrochemical Treatment of OrangeII Dye Solution-use of Aluminum Sacrificial Electrodes and Floc Characterization. J Hazard Mater. 2010;174:851-8.

19. Uddin MT, Islam MA, Mahmud S, Rukanuzzaman M. Adsorptive removal of methylene blue by tea waste. Journal of Hazardous Materials. 2009;164(1):53-60.

20. Gao H, Zhao S, Cheng X, Wang X, Zheng L. Removal of anionic azo dyes from aqueous solution using magnetic polymer multi-wall carbon nanotube nanocomposite as adsorbent. Chemical Engineering Journal. 2013;223:84-90.

21. Ighalo JO, Igwegbe CA, Aniagor CO, Oba SN. A Review of Methods for the Removal of Penicillins from Water. Journal of Water Process Engineering, 2021;39:101886.

22. Balarak D, Jaafari J, Hassani G, Mahdavi Y, Tyagi I, Agarwal S, Gupta VK. The use of low-cost adsorbent (Canola residues) for the adsorption of methylene blue from aqueous solution: Isotherm, kinetic and thermodynamic studies. Colloids and Interface Science Communications. 2015;7:16-9.

23. Bayram T, Bucak S, Ozturk D. BR13 dye removal using Sodium Dodecyl Sulfate modified montmorillonite: Equilibrium, Thermodynamic, Kinetic and Reusability studies. Chemical Engineering and Processing-Process Intensification, 2020;158:108186.

24. Ozturk D, Sahan T, Bayram T, Erkus A. Application of response surface methodology (RSM) to optimize the adsorption conditions of cationic basic yellow 2 onto pumice samples as a new adsorbent. Fresen. Environ. Bull, 2017,26:3285-5.

25. Ler A, Stanforth R. Evidence for surface precipitation of phosphate on goethite. Environmental Science & Technology. 2003;37(12):2694-700.

26. Zhou Q, Maurice PA, Cabaniss SE. Size fractionation upon adsorption of fulvic acid on goethite: Equilibrium and kinetic studies. Geochimica et Cosmochimica Acta. 2001;65(5):803-12.

27. Xie J, Gu X, Tong F, Zhao Y, Tan Y. Surface complexation modeling of Cr (VI) adsorption at the goethite–water interface. Journal of colloid and interface science. 2015;455:55-62.

28. Foroutan R, Mohammadi R, Adeleye AS, Farjadfard S, Esvandi Z, Arfaeinia H, Sorial GA, Ramavandi B, Sahebi S. Efficient arsenic (V) removal from contaminated water using natural clay and clay composite adsorbents. Environmental Science and Pollution Research. 2019;26(29):29748-62.

29. Dong Y, Yang H, Rao R, Zhang A. Selective synthesis of α-FeOOH and α-Fe2O3 nanorods via a temperature controlled process. Journal of Nanoscience and Nanotechnology. 2009;9(8):4774-9.

30. Ighalo JO, Adeniyi AG, Eletta OAA, Arowoyele LT. Competitive adsorption of Pb(II), Cu(II), Fe(II) and Zn(II) from aqueous media using biochar from oil palm (Elaeis guineensis) fibers: A Kinetic and equilibrium study. Indian Chemical Engineer. 2020:1-11.

31. Igwegbe CA, Onukwuli OD, Ighalo JO, Okoye PU. Adsorption of cationic dyes on Dacryodes edulis seeds activated carbon modified using phosphoric acid and sodium chloride. Environmental Processes. 2020;7(4):1151-71.

32. AbdurRahman FB, Akter M, Abedin MZ. Dyes removal from textile wastewater using orange peels. International journal of scientific & technology research. 2013;2(9):47-50.

33. Li F, Geng D, Cao Q. Adsorption of As (V) on aluminum-, iron-, and manganese-(oxyhydr) oxides: equilibrium and kinetics. Desalination and Water Treatment. 2015;56(7):1829-38.

34. Ighalo JO, Adeniyi AG. A Mini-Review of the Morphological Properties of Biosorbents Derived from Plant Leaves. SN Applied Sciences. 2020;2(3):509.

35. Ighalo JO, Adeniyi AG, Adelodun AA. Recent Advances on the Adsorption of Herbicides and Pesticides from Polluted Waters: Performance Evaluation via Physical Attributes. Journal of Industrial and Engineering Chemistry. 2020.

36. Özcan AS, Erdem B, Özcan A. Adsorption of Acid Blue 193 from aqueous solutions onto Na–bentonite and DTMA–bentonite. Journal of colloid and Interface science. 2004;280(1):44-54.

37. Erdem B, Özcan AS, Özcan A. Preparation of HDTMA-bentonite: Characterization studies and its adsorption behavior toward dibenzofuran. Surface and Interface Analysis. 2010;42(6-7):1351-6.

38. Özcan A, Ömeroğlu Ç, Erdoğan Y, Özcan AS. Modification of bentonite with a cationic surfactant: an adsorption study of textile dye Reactive Blue 19. Journal of hazardous materials. 2007;140(1-2):173-9.

39. Zhou Y, Jin X-Y, Lin H, Chen Z-L. Synthesis, characterization and potential application of organobentonite in removing 2, 4-DCP from industrial wastewater. Chemical engineering journal. 2011;166(1):176-83.

40. Şahan T, Öztürk D. Investigation of Pb (II) adsorption onto pumice samples: application of optimization method based on fractional factorial design and response surface methodology. Clean Technologies and Environmental Policy, 2014;16(5):819-831.

41. Mittal A, Krishnan L, Gupta V. Removal and recovery of malachite green from wastewater using an agricultural waste material, de-oiled soya. Separation and Purification Technology, 2005;43(2): 125-133.

42. Zazouli MA, Yazdani J, Balarak D, Ebrahimi M, Mahdavi Y. Removal Acid Blue 113 from aqueous solution by canola. J Mazandaran Univ Med Sci 2013;22(2):71-8.

43. Luo P, Zhao Y, Zhang B, Liu J, Yang Y, Liu J. Study on the adsorption of Neutral Red from aqueous solution onto halloysite nanotubes. Water research. 2010;44(5):1489-97.

44. Pekkuz H, Uzun I, Güzel F. Kinetics and thermodynamics of the adsorption of some dyestuffs from aqueous solution by poplar sawdust. Bioresource technology. 2008;99(6):2009-17.

45. Eletta OAA, Adeniyi AG, Ighalo JO, Onifade DV, Ayandele FO. Valorisation of Cocoa (Theobroma cacao) Pod Husk as Precursors for the Production of Adsorbents for Water Treatment. Environmental Technology Reviews. 2020;9(1):20-36.

46. Igwegbe CA, Oba SN, Aniagor CO, Adeniyi AG, Ighalo JO. Adsorption of Ciprofloxacin from Water: A Comprehensive Review. Journal of Industrial and Engineering Chemistry. 2020.

47. Baocheng Q, Jiti Z, Xiang X, Zheng C, Hongxia Z, Xiaobai Z. Adsorption behavior of Azo Dye CI Acid Red 14 in aqueous solution on surface soils. Journal of Environmental Sciences. 2008;20(6):704-9.

48. Langmuir I. The adsorption of gases on plane surfaces of glass, mica and platinum. Journal of the American Chemical society. 1918;40(9):1361-403.

49. Freundlich H. Over the adsorption in solution. J Phys Chem. 1906;57(385471):1100-7.

50. Temkin M, Pyzhev V. Recent modifications to Langmuir isotherms. Acta Physiochim URSS. 1940;12:217-22.

51. Dubinin MM, Radushkevich LV. Equation of the characteristic curve of activated charcoal. Proceedings of the Academy Sciences Physical Chemistry Section, USSR. 1947;55:331-3.

52. Gök Ö, Özcan AS, Özcan A. Adsorption behavior of a textile dye of Reactive Blue 19 from aqueous solutions onto modified bentonite. Applied surface science. 2010;256(17):5439-43.

53. Lagergren S, Svenska BK. On the theory of so-called adsorption of dissolved substances. The Royal Swedish Academy of Sciences Documents Band. 1898;24:1-13.

54. Ho YS, McKay G. Pseudo-second order model for sorption processes. Process Biochemistry. 1999;34:451–65.

55. Weber W, Morris J. Kinetics of adsorption on carbon from solution. J Sanit Eng Div Am Soc Civ Eng 1963;89:31-60.

56. Moussavi SP, MohammadianFazli M. Acid violet 17 Dye decolorization by multi-walled carbon nanotubes from aqueous solution. Journal of Human, Environment and Health Promotion. 2016;1(2):110-7.

57. Mohamed MM. Acid dye removal: comparison of surfactant-modified mesoporous FSM-16 with activated carbon derived from rice husk. Journal of Colloid and Interface Science. 2004;272(1):28-34.

58. Balarak D, Mostafapour FK. Adsorption of acid red 66 dye from aqueous solution by heat-treated rice husk. Research Journal of Chemistry and Environment. 2018;22(12):80-4.

59. Ighalo JO, Ajala JO, Umunweke G, Ogunniyi S, Adeyanju CA, Igwegbe CA, Adeniyi AG. Mitigation of Clofibric Acid Pollution by Adsorption: A Review of Recent Developments. Journal of Environmental Chemical Engineering. 2020;8(5):104264.

60. Inyinbor A, Adekola F, Olatunji GA. Kinetics, isotherms and thermodynamic modeling of liquid phase adsorption of Rhodamine B dye onto Raphia hookerie fruit epicarp. Water Resources and Industry. 2016;15:14-27.

61. Kuo CY, Wu CH, Wu JY. Adsorption of direct dyes from aqueous solutions by carbon nanotubes: Determination of equilibrium, kinetics and thermodynamics parameters. J Colloid Interface Sci. 2008;327(2):308–15.

62. Balarak D, Chandrika K, Igwegbe CA, Ahmadi S, Umembamalu CJ. Biosorption of phenol using modified barley husk: studies on equilibrium isotherm, kinetics, and thermodynamics of interactions. Sigma: Journal of Engineering & Natural Sciences/Mühendislik ve Fen Bilimleri Dergisi. 2020;38(3).

63. Eletta AAO, Tijani IO, Ighalo JO. Adsorption of Pb(II) and Phenol from Wastewater Using Silver Nitrate Modified Activated Carbon from Groundnut (Arachis hypogaea L.) Shells. West Indian Journal of Engineering. 2020;43(1):26-35.

64. Jung K-W, Choi BH, Hwang M-J, Jeong T-U, Ahn K-H. Fabrication of granular activated carbons derived from spent coffee grounds by entrapment in calcium alginate beads for adsorption of acid orange 7 and methylene blue. Bioresource Technology. 2016;219:185-95.

65. Yoon S, Calvo JJ, So MC. Removal of acid orange 7 from aqueous solution by metal-organic frameworks. Crystals. 2019;9(1):17.

66. Pan X, Zhang M, Liu H, Ouyang S, Ding N, Zhang P. Adsorption behavior and mechanism of acid orange 7 and methylene blue on self-assembled three-dimensional MgAl layered double hydroxide: Experimental and DFT investigation. Applied Surface Science. 2020:146370.

67. Jia L, Liu W, Cao J, Wu Z, Yang C. Modified multi-walled carbon nanotubes assisted foam fractionation for effective removal of acid orange 7 from the dyestuff wastewater. Journal of Environmental Management. 2020;262:110260.

68. Saeidi M, Biglari H, Rahdar S, Baneshi M, Ahamadabadi M, Narooie MR, et al. The adsorptive acid orange 7 using Kenya tea pulps ash from aqueous environments. Journal of Global Pharma Technology. 2017;9(4):13-9.

69. Nourmoradi H, Ghiasvand AR, Noorimotlagh Z. Removal of methylene blue and acid orange 7 from aqueous solutions by activated carbon coated with zinc oxide (ZnO) nanoparticles: equilibrium, kinetic, and thermodynamic study. Desalination and Water Treatment. 2014;55(1):252–62.

70. Silva JP, Sousa S, Rodrigues J, Antunes H, Porter JJ, Gonçalves I, et al. Adsorption of acid orange 7 dye in aqueous solutions by spent brewery grains. Separation and Purification Technology. 2004;40(3):309-15.

71. Jin X, Jiang M, Shan X, Pei Z, Chen Z. Adsorption of methylene blue and orange II onto unmodified and surfactant-modified zeolite. Journal of Colloid and Interface Science. 2008;328(2):243–7.

72. Lim CK, Bay HH, Neoh CH, Aris A, Majid ZA, Ibrahim Z. Application of zeolite-activated carbon macrocomposite for the adsorption of Acid Orange 7: isotherm, kinetic and thermodynamic studies. Environmental Science and Pollution Research. 2013;20(10):7243-55.

73. Hevira L, Zilfa, Rahmayeni, Ighalo JO, Aziz H, Zein R. Terminalia catappa shell as low-cost biosorbent for the removal of methylene blue from aqueous solutions. Journal of Industrial and Engineering Chemistry, 2021.

74. Ighalo JO, Igwegbe CA, Adeniyi AG, Adeyanju CA, and Ogunniyi S, Mitigation of Metronidazole (Flagyl) Pollution in Aqueous Media by Adsorption: A Review. Environmental Technology Reviews, 2020; 9(1):137-148.

Ultimate Eradication of Acid Orange 7 from Contaminated Liquid via Synthesized Mesoporous Goethite

Davoud Balarak, Fatemeh Ganji, Periakaruppan Rajiv, Chinenye Adaobi Igwegbe*, Joshua O. Ighalo

SUPPLEMENTARY INFORMATION

MPG preparation

The mesoporous goethite was synthesized by the oxidation of ferrous sulfate heptahydrate with hydrogen peroxide in aqueous solution following the method reported by Dong et al. (2009). Typically, 0.70 g ferrous sulfate heptahydrate were added to 21.0 g ultrapure water, and then 30% hydrogen peroxide (6.0 mL) was added to the above-mentioned solution under vigorous stirring to obtain a homogeneous yellow slurry solution. Then the suspension was transferred into a PTFE lined hydrothermal synthesis reactor maintaining 150 °C for 6 h. At last, the solid product was centrifuged and rinsed with ultrapure water for several times until the supernatant was near neutral and dried overnight at 80 °C under vacuum.

Regeneration of used MPG

In this study, the used MPG was regenerated by NaCl solution (1 M) treatment, since the “NaCl regeneration” method stood out in all methods (Erdem et al. 2010). In the regeneration process, the used MPG was mixed with 1 M NaCl solution. Then, the mixture was stirred at 200 rpm at 25 °C for 2 h and the regeneration was performed 8 steps. Finally, the solid samples were filtered, washed, dried and sieved through a 100 mesh for further analysis. And comparison was made between the AO7 uptake capacity obtained using regenerated samples and with those obtained using fresh MPG ones.